http://dx.doi.org/10.5012/bkcs.2011.32.9.3317

Synthesis of Zr-incorporated TiO_2 Using a Solvothermal Method and its Photovoltaic Efficiency on Dye-sensitized Solar Cells

Sujung Kim and Misook Kang*

Department of Chemistry, College of Science, Yeungnam University, Gyeongsan, Gyeongbuk 712-749, Korea
**E-mail: mskang@ynu.ac.kr*
Received May 17, 2011, Accepted July 20, 2011

This study examines the photoelectric conversion efficiency of dye-sensitized solar cells (DSSCs) when nanometer-sized Zr (0.1, 0.5, and 1.0 mol %)-TiO_2 prepared using a solvothermal method is utilized as the working electrode material. The particle sizes observe in the transmission electron microscopy (TEM) images are < 30 nm in all samples. The absorption band is slightly broadened at the tail for the 0.1 mol % Zr-TiO_2, and the intensity of the photoluminescence (PL) curves of the Zr-incorporated TiO_2 is significantly smaller than that of the pure TiO_2. Compared to that using pure TiO_2, the energy conversion efficiency is enhanced considerably by the application of Zr-TiO_2 in the DSSCs to approximately 6.17% for 0.5 mol % Zr-TiO_2 with the N719 dye (10.0 μm film thickness and 5.0 mm × 5.0 mm cell area) under 100 mW/cm^2 of simulated sunlight.

Key Words : Solvothermal method, Zr-TiO_2, Dye-sensitized solar cells, Energy conversion efficiency, Impedance, Photoluminescence

Introduction

Dye-sensitized solar cells (DSSCs) consist of a sensitizing dye, transparent conducting substrates (fluorine-doped tin oxide; FTO), nanometer-sized TiO_2 film, iodide electrolyte, and counter electrode (Pt or carbon). As a dye molecule absorbs light, the electrons on the highest occupied molecular orbital (HOMO) are excited to an electronically excited state: the lowest unoccupied molecular orbital (LUMO). The excited dye molecule injects an electron into the conducting band of the TiO_2 film. The oxidized dye is restored by electron donation from the reducing ions in the electrolyte, usually an organic solvent containing a redox system. The donated electron is in turn regenerated by the reduction of conjugated ions in the electrolytes. The circuit is competed by electron migration through an external load.[1-5]

Nano-crystalline titanium dioxide, as a core material in DSSCs, has been studied extensively as an anode electrode on account of its interesting physical and chemical properties, particularly its redox reaction surface.[6-8] The optical efficiency of meso (nano) porous TiO_2 has recently been reported to be approximately 0.5 to 1.0% higher than that of existing nanoparticles.[9-12] Although, nano-sized Sn and Zn oxides with a slightly higher band gap than pure TiO_2, which can improve the electron donating/accepting between the semiconductor and LUMO energy levels of the dye, have been examined, there are a few reports of performance degradation.[13,14] Therefore, continued efforts to find excellent metal oxides are needed.

In order to enhance the photovoltaic efficiency, electrons, which are transferred from the LUMO of dye molecules, should be accepted easily and donated to the external surface of the semiconductor film. However, a limitation is imposed by the loss of electrons that are moved and then dropped down onto a spherical surface of a semiconductor film. The electron is expected to migrate rapidly to the surface of a defected semiconductor film that is well-arranged by self assembly with electron capturing and donating properties and converted into an FTO-conducting electrode without electron loss, thereby increasing the energy conversion efficiency. Promising metals with good electron capturing and donating properties included In,[15] Ga,[16] and Zr.[17] In particular, Kitiyanan *et al.*[17] reported a zirconium effect in the DSSC assembled by 95 mol % mesoporous TiO_2-5 mol % ZrO_2 composite based on a sol-gel method. Their cell fabricated by 5-μm-thick mixed TiO_2-ZrO_2 electrode had a short-circuit photocurrent density (J_{sc}) of about 13 mAcm^{-2}, open-circuit voltage (V_{oc}) of about 600 mV and conversion efficiency of 5.4%. They concluded that the Brunauer, Emmett and Teller (BET) surface area of 95:5 mol % TiO_2-ZrO_2 mixed oxides, at 109 m^{2}g^{-1}, is about 35% higher than TiO_2, and consequently it exerted a greater effect on the photovoltaic efficiency in DSSC. However, they did not describe the effects of nano-sized titania use, Zr concentration, and the Zr substitution into framework. More detailed study is thus required.

In contrast to these previous papers, this study therefore used a solvothermal method to introduce Zr ions at various concentrations into the TiO_2 tetrahedral framework (Zr-TiO_2) for application to DSSC. The synthesized samples were characterized by X-ray diffraction (XRD), transmission electron microscopy (TEM), photoluminescence (PL), UV-visible spectroscopy, and impedance analysis. The photovoltaic performance of the Zr-TiO_2/dye (N719) solar cell was evaluated from the overall conversion efficiency, fill factor (FF), V_{oc} and J_{sc}. In addition, the efficiency was compared with that of a pure TiO_2 sample prepared using the

same synthesis method.

Experimental

Preparation of Zr-TiO_2s. Zr-TiO_2 with various mol fractions of zirconium (0.1, 0.5, and 1.0 mol %) was prepared using a solvothermal method.[18] Titanium tetraisopropoxide (TTIP, 99.95%, Junsei Chemical, Tokyo, Japan) and zirconium chloride ($ZrCl_4$, 99.99%, Junsei Chemical, Tokyo, Japan) were used as the titanium and zirconium precursors, respectively. Ethanol was used as the solvent. After 0.1, 0.5, and 1.0 mol % of zirconium chloride and 1.0 mol TTIP were added stepwise to 250 mL of ethanol, the mixture was stirred homogeneously for 2 h. Acetic acid was added and the pH was maintained at 3.0 for rapid hydrolysis. The final solution was stirred homogeneously for 2 h and moved to an autoclave for thermal treatment. TTIP and zirconium chloride were hydrolyzed during thermal treatment at 200 ºC for 8 h under a nitrogen environment with a pressure of approximately 15.0 atm. The resulting precipitate was washed with distilled water until the pH was neutralized at 7.0 and then dried at 80 ºC for 24 h.

Characteristics of Zr-TiO_2s. The synthesized Zr-TiO_2 powders were examined by XRD (MPD, PANalytical, at Yeungnam University Instrumental Analysis Center) with nickel-filtered CuKα radiation (30 kV, 30 mA) at 2θ angles ranging from 10 to 80º, a scan speed of 10º min^{-1} and a time constant of 1 s.

The sizes and shapes of the Zr-TiO_2 particles were measured by TEM (H-7600, Hitachi, at Yeungnam University Instrumental Analysis Center) operated at 120 kV.

The BET surface areas of the Zr-TiO_2 powders were measured by nitrogen gas adsorption using a continuous flow method. A chromatograph (Micromeritics Gemini 2375; Londonderry, NH, USA) equipped with a thermal conductivity detector at liquid-nitrogen temperature was used. A mixture of nitrogen and helium was used as the carrier gas. The sample was treated at 350 °C for 3 h before nitrogen adsorption.

The conductivity (resistance) is expressed in ohms per square unit, and was estimated using a SIMCO Trustat Work Surface Tester (Model ST-3, Japan). The apparatus accurately measures the resistance within the range of 102 to 1,012 Ω per square unit for a potential difference (V) of 15 V between the parallel conductive probes, and can also deliver a current up to 1.5 mA. These current (I) measurements were used to determine the surface resistance. The resistance between the probes (R) in the test was calculated automatically from Ohm's law: R=V/I. The arrangement of the probes (opposite sides of a square) made the resistance measurements in ohms equivalent to the surface resistance in ohms per square unit. The resistance of the pure PET film was 9.0 × 1,010 Ω per square unit.

The UV-visible spectra were obtained using a Cary 500 spectrometer with a reflectance sphere over the special range of 200 to 800 nm.

PL spectroscopy was also performed to determine the number of photo-excited electron hole pairs using a PL mapping system (LabRamHR, Jobin Yvon, at Korea Photonics Technology Institute Material Characterization Center). It was also used to examine the number of photo-excited electron-hole pairs for all samples. Samples of 1.0-mm diameter pellets were measured at room temperature using a He-Cd laser source at 325 nm in the reflection mode.

AC impedance measurements were performed with the potentiostat-galvanostat equipped with a compactstat electrochemical interface from IVIUM technology under constant light illumination of 100 $mWcm^{-2}$. Impedance measurements where performed at frequencies between 0.1 and 100 kHz with an ac signal of 10 mV amplitude. The applied bias voltage and ac amplitude were set at V_{oc} of the DSSC. One sun illumination was obtained from a 100 W xenon lamp.

Manufacturing Dye-sensitized Solar Cells (DSSCs). To prepare the Zr-TiO_2 thin film, a paste was produced by mixing 2.0 g of nanometer-sized Zr-TiO_2 powders with a mixture consisting of 5.0 g of α-tepinol, 0.5 g of cellulose, and 20 mL of ethanol, after sonication for 24 h at 1200 Wcm^{-2}. A Zr-TiO_2 film was fabricated by coating onto an FTO conducting glass plate (Hartford FTO, ~30 $ohmcm^{-2}$, 80% transmittance in visible region) using a squeeze printing technique. The film was treated by heating at 450 ºC for 30 minutes to remove the additives. For DSSC manufacture, the prepared thin film electrode was immersed in a 3.0×10^{-4} M N719 dye solution at room temperature for 2 h, rinsed with anhydrous ethanol and dried. A Pt-coated FTO electrode was placed over the dye-adsorbed Zr-TiO_2 electrode, and the edges of the cell were sealed with a sealing sheet (PECHM-1, Mitsui-Dupont Polychemical). The redox electrolyte consisted of 0.5 mol KI, 0.05 mol I_2, and 0.5 mol 4-tert-butylpyridine as a solvent. The photocurrent-voltage (I-V) curves were used to calculate the J_{sc}, V_{oc}, FF, and overall conversion efficiency of the DSSCs. The I-V curves were measured under white light irradiation from a xenon lamp (max. 150W, Newport). The incident light intensity and active cell area were 100 $mWcm^{-2}$ and 0.25 (0.5 cm × 0.5 cm) cm^2, respectively.

Results and Discussion

Characteristics of Zr-TiO_2s. Figure 1 shows the XRD patterns of the 0.1, 0.5, and 1.0 mol % Zr-TiO_2 nanometer-sized powders, and pure TiO_2. Without thermal treatment above 500 ºC, the Zr-TiO_2 particles exhibited a pure anatase structure. The anatase structure showed peaks at 25.3, 38.0, 48.2, 54, 63, and 68° 2θ, which were assigned to the (d_{101}), (d_{004}), (d_{200}), (d_{105}), (d_{211}), and (d_{204}) planes, respectively.[19] The absence of any peaks assigned to ZrO_2 indicated the good incorporation of the Zr ions into the anatase framework. However, the peak intensity at most of the planes in Zr-TiO_2 decreased slightly with increasing zirconium content, compared to that of pure TiO_2. Generally, the crystalline domain sizes decrease with increasing line-broadening of the peaks. The line broadening of the peak of the A (101) index is related to the size of the hexagonal crystalline

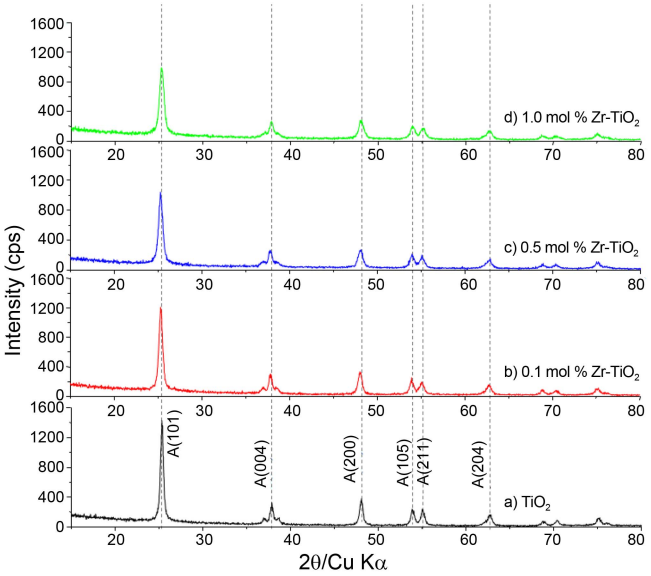

Figure 1. XRD patterns of pure TiO_2 and Zr-TiO_2 synthesized by solvothermal method.

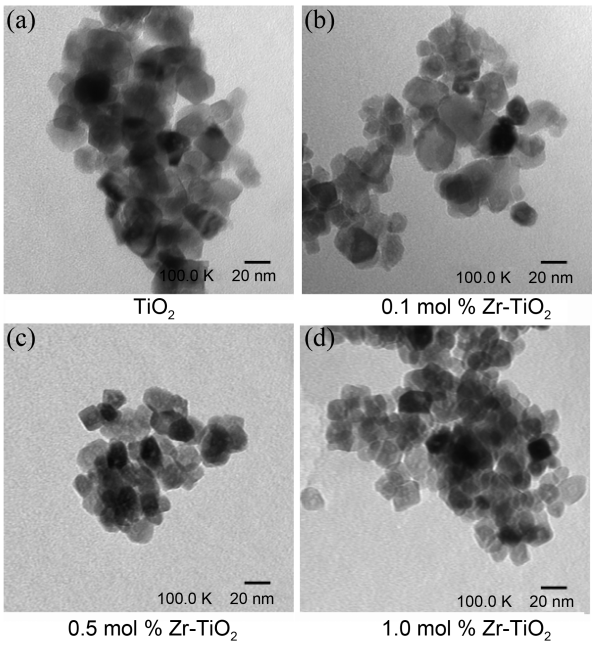

Figure 2. TEM images of pure TiO_2 and as-synthesized Zr-TiO_2.

phase. Scherrer's equation,[20] $t = 0.9\lambda/\beta\cos\theta$, where λ is the wavelength of the incident X-rays, β the full width at half maximum (FWHM) height in radians, and θ the diffraction angle, was used to estimate the crystalline domain size. When the FWHM of the peak at 25.3° 2θ was selected, the calculated crystalline domain sizes were 33, 27, 25, and 21 nm for TiO_2 and 0.1, 0.5, and 1.0 mol % Zr-TiO_2, respectively.

Figure 2 shows TEM images of the particle shapes of TiO_2 and 0.1, 0.5, and 1.0 mol % Zr-TiO_2. A relatively uniform mixture of rhombic and cubic particles with sizes ranging from 20 to 30 nm was observed. When zirconium was added, the particles were slightly decreased in size, in the order of pure TiO_2 < 0.1 mol % Zr-TiO_2 > 0.5 mol % Zr-TiO_2 = 1.0 mol % Zr-TiO_2. This corresponds to the XRD patterns shown in Figure 1.

Table 1 summarizes the specific surface area and conductivity of the Zr-TiO_2 powders, and the atomic compositions on the external surface at the specified portion of the square in the figure below the table. The BET surface areas increased with increasing Zr content. Generally, the surface area is strongly and inversely correlated to the particle size. The transferring electron is very important for enhancing the photoelectric efficiency in DSSC. Therefore, this study examined the surface conductivity of the Zr-TiO_2 film. The conductivity (ohm(Ω)cm^{-2}(□)) was better on the 0.5 mol % Zr-TiO_2 film (1.0×10^8 Ωcm^{-2}).

Table 1. Specific surface areas and conductivity of pure TiO_2 and as-synthesized Zr-TiO_2

Element / Materials	Atomic ratio (%)			Specific surface area (m^2g^{-1})	Conductivity (Ωcm^{-2})
	Zr	Ti	O		
TiO_2	0.00	31.15	68.85	65	2.0×10^{10}
0.1 mol % Zr-TiO_2	0.00	26.48	73.52	68	1.0×10^9
0.5 mol % Zr-TiO_2	0.15	22.12	77.72	77	1.0×10^8
1.0 mol % Zr-TiO_2	0.31	28.03	71.66	76	2.0×10^8

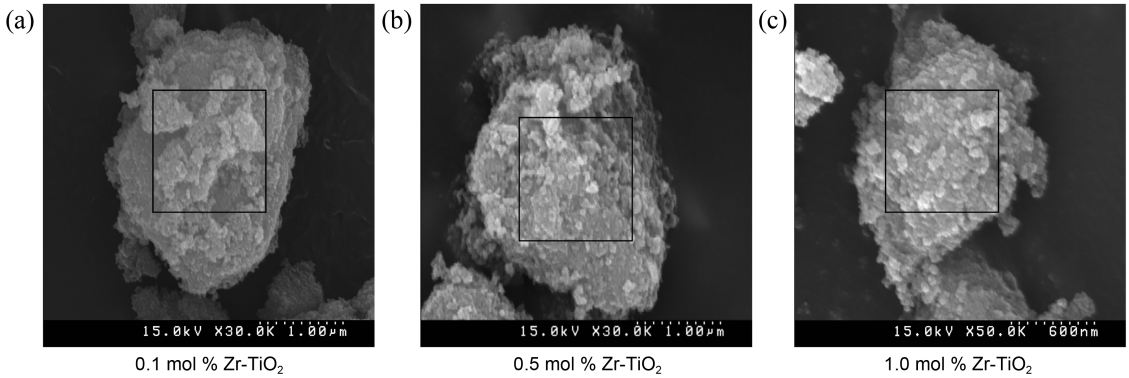

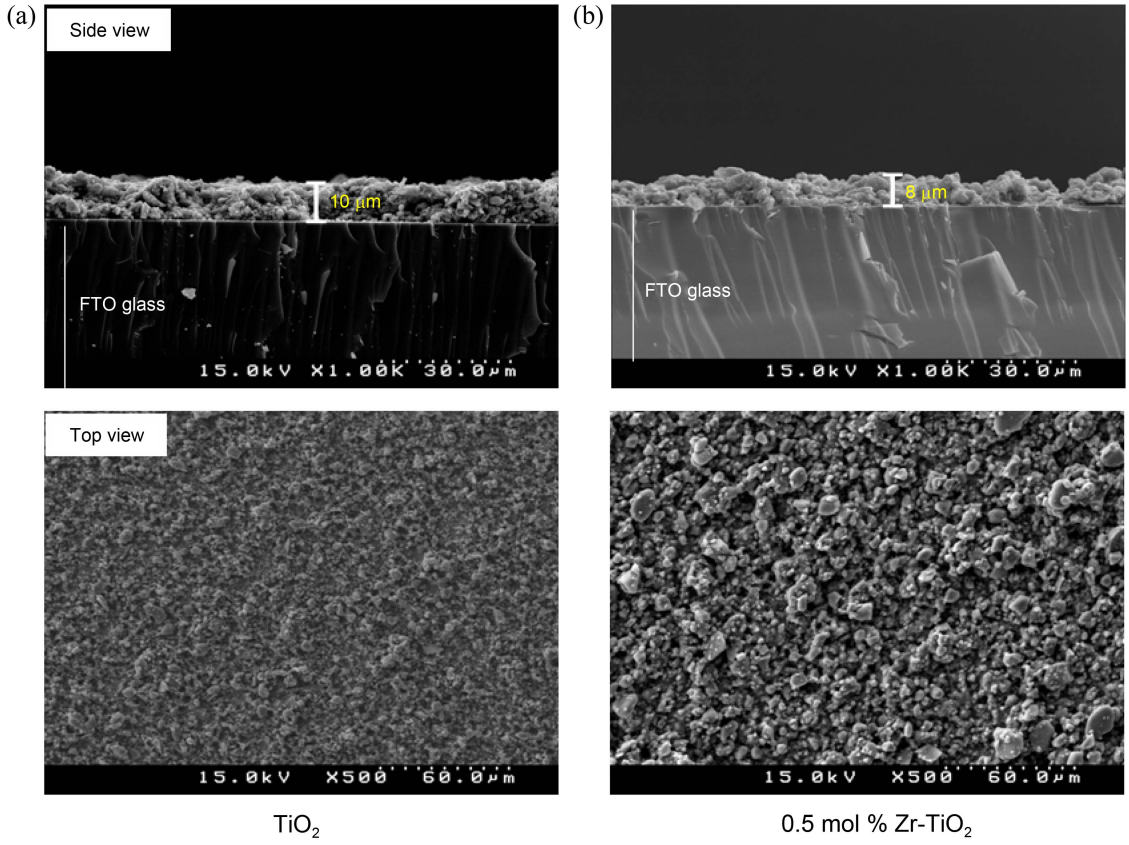

Figure 3. Film thickness and morphology in SEM photos of pure TiO_2 and Zr-TiO_2 films.

Photovoltaic Performance of Zr-TiO_2s. The photoelectric properties were measured using a voltmeter and ampere meter (Model 2000, Keithley) with a variable load. The voltmeter above power failure and a lock-in amplifier were used. A 150 W illuminant Xenon lamp was employed as a radiation source at an AM-1.5 radiation angle. The light intensities were measured using a power analyzer and thermal smart-sensor. The FF and solar energy conversion efficiency (η) were calculated according to Equations (1) and (2), respectively.[21,22]

$$\mathbf{FF} = I_{max} \times V_{max}/I_{sc} \times V_{oc} \quad (1)$$

$$\boldsymbol{\eta}\ \mathbf{(\%)} = P_{out}/P_{in} \times 100 = I_{max} \times V_{max}/P_{in} \times 100 = I_{sc} \times V_{oc} \times FF \quad (2)$$

Figure 3 present the morphology at the top view and film thickness at the side view for TiO_2 and 0.5 mol % Zr-TiO_2 films. Despite being made with the same amounts, the film depths differed at 10 and 8 mm, respectively, which was attributed to the difference of particle size. However, despite the smaller particle size of the Zr-TiO_2 films, the morphology at the top view indicated a rougher surface with many pores. This result suggested that the dye will be well adsorbed on the Zr-TiO_2 film, similar to mesoporous titania.[11]

Figure 4 shows the photocurrent-voltage curves of pure TiO_2 and Zr-TiO_2 synthesized using a solvothermal method. The FF, V_{oc}, J_{sc}, and overall energy efficiency were determined as described above. The film thickness was in the range of 8.0-10.0 mm and the unit cell area was fixed with dimensions of 5.0 mm × 5.0 mm. A DSSC assembled with pure TiO_2 had a V_{oc} of 0.66 V and a J_{sc} of 7.49 mAcm^{-2} at an incident light intensity of 100 mW/cm^2. The power conversion efficiency was 3.85% for the pure TiO_2 anatase structure, but increased to 6.17% in the DSSC made from 0.5 mol % Zr-TiO_2 film, with a J_{sc} of 12.60 mAcm^{-2}. As shown in the right figure, the colors on the pure TiO_2 and Zr-TiO_2 film were changed to dark pink and brown, respectively, after adsorption of N719 dye, which was attributed to the amount of N719 adsorbed onto the film surface. On the other hand, the efficiency was slightly reduced in the DSSC made with a Zr content > 1.0 mol %, which confirmed that Zr-TiO_2 is a better material in DSSC than pure TiO_2.

All the impedance spectra shown in Figure 5 illustrated three semicircles in the measured frequency range of 0.1-100 kHz. Notably, R_h, the ohmic serial resistance, is associated with the series resistance of the electrolytes and electric contacts in the DSSC. R_1, the charge transfer resistance, occurs at the Pt counter-electrode. R_2 has been associated with the resistance at the TiO_2 (semi-conducting electrode)/dye/electrolyte interface, whereas R_3 has been associated with the Nernstian diffusion within the electrolytes.[23,24] All the measured impedance data for the two types of DSSC are also included in the table under the figure. The pure TiO_2-DSSC appeared to have higher total resistances in the current path across the device than the 0.5 mol % Zr-TiO_2-DSSC. Notably, R_2, which means the resistance at the TiO_2/

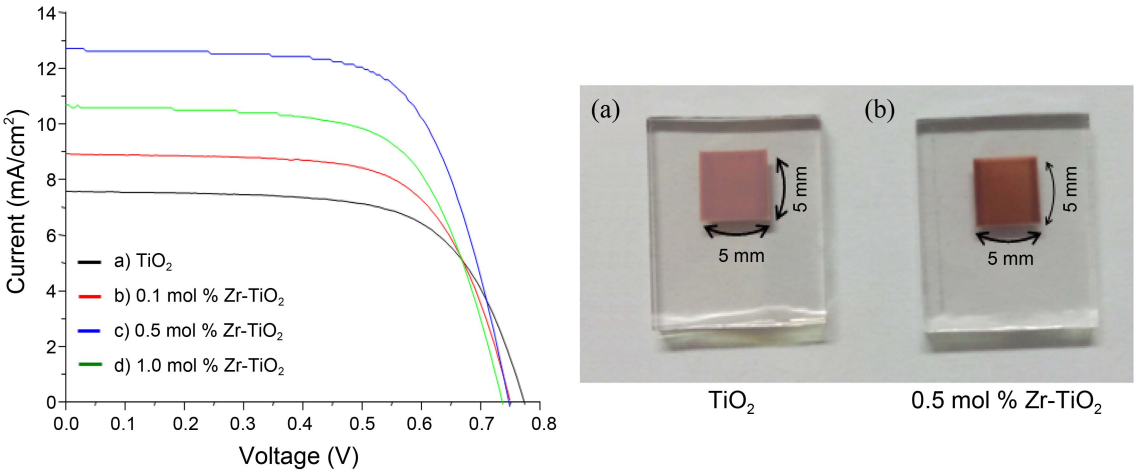

Working electrode	Dye	V_{oc} (V)	J_{sc} (mAcm^{-2})	Fill factor	Efficiency (%)
a) TiO_2	N719	0.78	7.49	0.66	3.85
b) 0.1 mol % Zr-TiO_2	N719	0.76	8.95	0.66	4.45
c) 0.5 mol % Zr-TiO_2	N719	0.75	12.60	0.65	6.17
d) 1.0 mol % Zr-TiO_2	N719	0.73	10.30	0.64	4.87

Figure 4. Solar energy conversion efficiency of the DSSCs fabricated with pure TiO_2 and Zr-TiO_2.

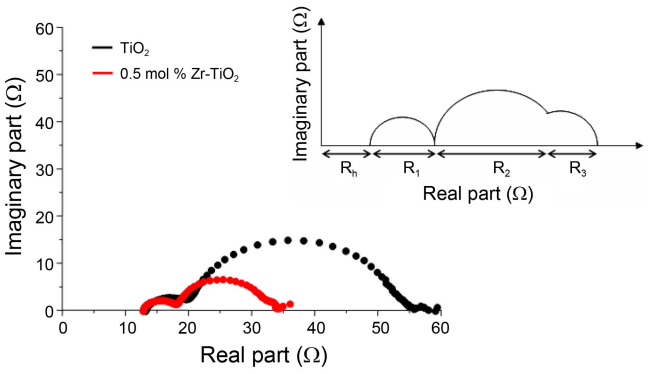

Working electrode	R_h (Ω)	R_1 (Ω)	R_2 (Ω)	R_3 (Ω)
TiO_2	13.2	6.3	36.2	2.3
0.5 mol % Zr-TiO_2	12.8	5.3	15.8	0.6

Figure 5. UV-visible spectra of pure TiO_2 and Zr-TiO_2.

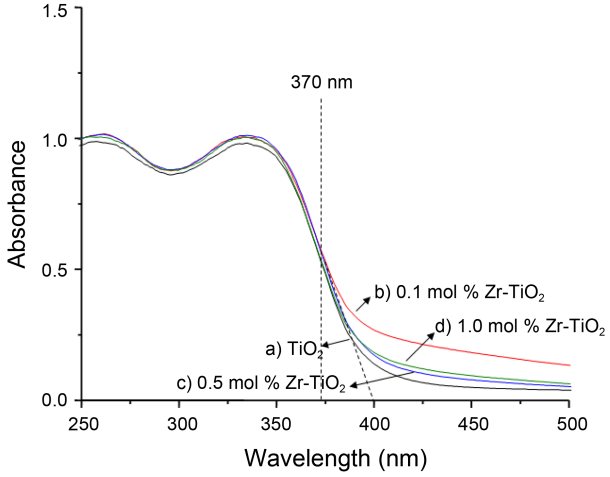

Figure 6. PL spectra of pure TiO_2 and Zr-TiO_2.

dye/electrolyte interface, was largely decreased in the cell assembled by 0.5 mol % Zr-TiO_2 compared to that of pure TiO_2. This confirmed the easy electron transfer over the Zr-TiO_2 surface, the significant flow amounts, and the capability of the Zr-TiO_2 to enhance the photocurrent and powder efficiency of DSSCs.

Optical Properties of Zr-TiO_2s. The UV-visible spectra of the Zr-TiO_2 powders were obtained to determine the relationship between the solar energy conversion efficiency and the spectroscopic property, as shown in Figure 6. The absorption band for the tetrahedral symmetry of Ti^{4+} normally appears at approximately 350-380 nm. In the spectra of Zr-TiO_2, the absorption bands were slightly shifted to a longer wavelength compared to pure TiO_2, and the broadened tail may indicate a Zr component. The band gap obtained by extrapolation in pure TiO_2 and 0.5 mol % Zr-TiO_2 was about 3.127 and 3.119 eV, respectively. The band gaps in a semiconductor material are closely related to the wavelength range absorbed, where the band gap decreases with increasing absorption wavelength. As TiO_2 plays the important roles of electron-receiving and -giving in DSSC, and its light absorption is therefore important, the electron transfer is more crucial to enhance the DSSC performance.

Figure 7 shows the PL spectra of Zr-TiO_2s. The PL curve suggests that the electrons in the valence band were transferred to the conduction band, and the excited electrons were then stabilized by photoemission. In general, it is very important that the PL intensity increases with the increasing number of emitted electrons resulting from recombination between excited electrons and holes, and, consequently, that the photo-activity decreases.[25] In particular, the PL intensity

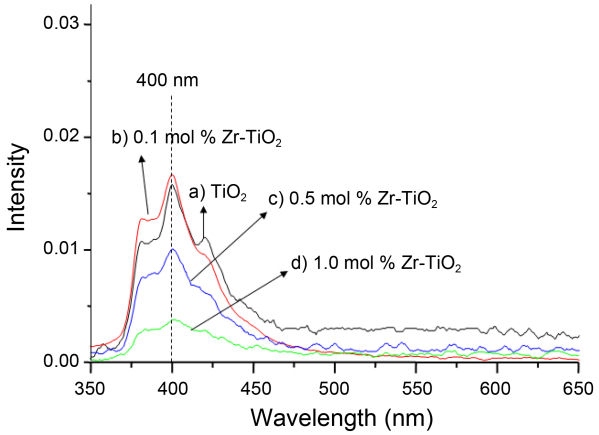

Figure 7. Impedance curves of the DSSCs fabricated with pure TiO_2 and Zr-TiO_2.

decreases to a greater extent in the presence of a metal that can capture excited electrons or exhibit conductivity, *via* the relaxation process. The PL curve of pure TiO_2 showed emission at 370-450 nm with a peak at 400 nm. The band broadening was attributed to the overlapped emission from the higher and lower excited states to the ground states. The curve pattern of Zr-TiO_2 was the same as that of pure anatase TiO_2. However, the PL intensity decreased significantly with increasing Zr concentration, which was most likely due to the electron capturing and releasing actions of the Zr atoms. This can encourage the transferring process to the transparent conducting oxide (TCO), leading to easier electron transfer activities. Consequently, the PL intensity varied according to whether the added metal acts as an electron capturer or not.

Conclusions

Zr-incorporated TiO_2 was prepared using a solvothermal method to enhance the solar energy conversion efficiency. In comparing the performance with that of pure TiO_2, the 0.5 mol % Zr-TiO_2 DSSC showed superior solar energy conversion efficiency. In 100 $mWcm^{-2}$ simulated sunlight, the 0.5 mol % Zr-TiO_2 DSSC exhibited good performance with a solar energy conversion efficiency of approximately 6.17%, V_{oc} of 0.75V, J_{sc} of 12.60 $mAcm^{-2}$, and FF of 0.65. The intensity of the PL curve of the Zr-incorporated TiO_2 was significantly decreased compared to that of pure TiO_2, which was related to the increased electron capturing that consequently increased the number of electrons being transferred to the transparent conducting glass (FTO). In addition, the resistance on the DSSC film was explained by impedance. The resistance was the smallest on 0.5 mol % Zr-TiO_2-DSSC, so that the photovoltaic performance was significantly improved with Zr addition to TiO_2.

Acknowledgments. This work was supported by the National Research Foundation of Korea (NRF) grant funded by the Korea government (MEST) (No. 2010-0015264), for which the authors are very grateful.

References

1. O'Regan, B.; Grätzel, M. *Nature* **1991**, *353*, 737.
2. Cahen, D.; Hodes, G.; Gra1tzel, M.; Guillemoles, J. F.; Riess, I. *J. Phys. Chem. B* **2000**, *104*, 2053.
3. Grätzel, M. *Comptes Rendus Chimie* **2006**, *9*, 578.
4. Bisquert, J.; Cahen, D.; Hodes, G.; Ru1hle, S.; Zaban, A. *J. Phys. Chem. B* **2004**, *108*, 8106.
5. Grätzel, M. *Nature* **2001**, *414*, 338.
6. Lee, Y.; Chae, J.; Kang, M. *J. Ind. Eng. Chem.* **2010**, *16*, 609.
7. Huang, C. Y.; Hsu, Y. C.; Chen, J. G.; Suryanarayanan, V.; Lee, K. M.; Ho, K. C. *Sol. Energy Mater. Sol. Cells* **2006**, *90*, 2391.
8. Haque, S. A.; Tachibana, Y.; Willis, R. L.; Moser, J. E.; Gra1tzel, M.; Klug, D. R.; Durrant, J. R. *J. Phys. Chem. B* **2000**, *104*, 538.
9. Jung, H. G.; Kang, Y. S.; Sun, Y. K. *Electrochimica Acta* **2010**, *55*, 4637.
10. Ngamsinlapasathian, S.; Sreethawong, T.; Suzuki, Y.; Yoshikawa, S. *Sol. Energy Mater. Sol. Cells* **2005**, *86*, 269.
11. Lee, Y.; Kang, M. *Mater. Chem. Phys.* **2010**, *122*, 284.
12. Zhang, Y.; Xie, Z.; Wang, J. *Thin Solid Films*, in press.
13. Lu, L.; Li, R.; Fan, K.; Peng, T. *Solar Energy* **2010**, *84*, 844.
14. Fukai, Y.; Kondo, Y.; Mori, S.; Suzuki, E. *Electrochem. Commun.* **2007**, *9*, 1439.
15. Jeon, M. K.; Kang, M. *Mater. Letters* **2008**, *62*, 676.
16. Chae, J.; Lee, J.; Jeong, J. H.; Kang, M. *Bull. Korean Chem. Soc.* **2009**, *30*, 302.
17. Kitiyanan, A.; Ngamsinlapasathian, S.; Pavasupree, S.; Yoshikawa, S. *J. Solid State Chem.* **2005**, *178*, 1044.
18. Kang, M. *Mater. Letters* **2005**, *59*, 3122.
19. Howard, C. J.; Sabine, T. M.; Dickson, F. *Acta Cryst. B* **1991**, *47*, 462.
20. Jian, Z.; Hejing, W. *Chinese J. Geochem.* **2003**, *22*, 38.
21. Vlachopoulos, N.; Liska, P.; Augustynski, J.; Grätzel, M. *J. Am. Chem. Soc.* **1988**, *110*, 1216.
22. Kalyanasundaran, K.; Grätzel, M. *Coord. Chem. Rev.* **1998**, *77*, 347.
23. Shin, I.; Seo, H.; Son, M. K.; Kim, J. K.; Prabakar, K.; Kim, H. J. *Curr. Appl. Phys.* **2010**, *10*, 422.
24. Wang, Q.; Moser, J. E.; Grätzel, M. *J. Phys. Chem. B* **2005**, *109*, 14945.
25. Baiju, K. V.; Zachariah, A.; Shukla, S.; Biju, S.; Reddy, M. L. P.; Warrier, K. G. K. *Catal. Lett.* **2009**, *130*, 130.